Transactions Papers

Anti-Collision Backscatter Sensor Networks

Aggelos Bletsas, *Member, IEEE*, Stavroula Siachalou, and John N. Sahalos, *Fellow, IEEE*

***Abstract*—Sensor collision (interference) is studied in a large network of low bit-rate sensors that communicate via backscatter, i.e. modulate the reflection of a common carrier transmitted by a central reader. Closed-form analysis is provided, quantifying sensor collision (interference) in high-density, backscatter sensor networks (BSN), as a function of number of tags and aggregate bandwidth. Analysis is applicable to a broad class of sensor subcarrier modulations, propagation environments and reader antenna directivity patterns. It is discovered that anti-collision performance in high-density backscatter sensor networks is feasible provided that appropriate modulation is used at each sensor. That is due to the round-trip nature of backscatter communication as well as the extended target range, which both impose stringent requirements on spectrum efficiency, not easily met by all modulations. Furthermore, aggregate bandwidth savings for given anti-collision performance are quantified, when simple division techniques on subcarrier (modulating) frequency and space (via moderately directive hub antenna) are combined.**

***Index Terms*—RFID, collision, outage probability, wireless networks.**

I. Introduction

MODULATION of power reflected by a single antenna has grounded the basis of backscatter communication and has had a long history [1]. Backscatter communication is nowadays extensively used in radio frequency identification systems (RFID), usually restricted in short-range applications. Typical scenarios include toll payments, electronic anti-theft surveillance, digital supply chain monitoring, smart cards, document tracking, medication pedigree or even interfaces for musical instruments [2],[3].

Manuscript received June 20, 2008; revised October 31, 2008; accepted July 6, 2009. The associate editor coordinating the review of this paper and approving it for publication was C. Tellambura.

S. Siachalou is with the General Directorate of Technical Services and Computerization, Aristotle Univ. of Thessaloniki (e-mail: ssiachal@ad.auth.gr).

J. N. Sahalos is with the Radiocommunications Laboratory (RCL), Dept. of Physics, Aristotle Univ. of Thessaloniki (e-mail: sahalos@auth.gr).

A. Bletsas was with RCL. He is now with the Telecom Laboratory, Electronic and Computer Engineering Dept., Technical Univ. of Crete (e-mail: aggelos@media.mit.edu, aggelos@telecom.tuc.gr).

This work was implemented in the context of Telecommunications Platform of Innovation Pole of C.M. Greece, through the O.P. Competitiveness 3rd Community Support Program and was funded from the Hellenic State-Ministry of Development-General Secretariat for Research and Technology. Parts of this work were presented in European Microwave Conference 2008, Amsterdam.

Digital Object Identifier 10.1109/TWC.2009.080834

Despite its typical short-range nature, backscatter communication was recently proposed for extended-range communication in sensor networks. Specifically, it was experimentally shown that modulating the reflection coefficient of a simple antenna, can be used for *low* bit-rate sensor communication with simple, software-defined radio [4], [5]. The sensor transceiver consists of a single transistor connected to an antenna that switches on/off at a specific subcarrier frequency. That operation modulates the reflection of a carrier transmitted by a central hub. In that way, each sensor transceiver becomes extremely ultra-low cost and low-power, since energy spent for communication is restricted to the energy used for switching on/off a transistor for modulation purposes, without any requirements for signal conditioning (e.g. filtering, amplification). Range restrictions, inherent in backscatter communication are bypassed with: a) utilization of each sensor's battery, already present and necessary for the sensing electronics (e.g. measuring acidity, humidity, or temperature) and b) ultra low-bit rate, on the order of tens of bits per second, allowing for extended energy per bit.

Anti-collision among multiple sensors that communicate via backscatter with a central hub becomes a major technical challenge in many relevant applications. Typical solutions include a receiver structure at each sensor and utilization of specific anti-collision algorithms categorized in two broad classes: a) tree-based algorithms that grant access to sensors with appropriate ID that matches the transmitted (from the hub) code suffix, and b) customized carrier sense multiple access (CSMA) algorithms that provide statistical time-divided access. Tree-based anti-collision is utilized in industry-adopted standards such as UHF EPC Class 0 and Class 1 while combination of tree-based and CSMA algorithms can be found in Class 1, Generation 2 [6], [7].

Nevertheless, the extended duration per information bit assumed in this work (on the order of hundreds of milliseconds), necessary for extended backscatter radio range (on the order of several tens of meters), precludes the use of tree-based or CSMA anti-collision variants, as the latter could provide for a large number of tag reads per second, only when symbol (bit) duration is limited (currently on the order of microseconds in EPC Class 0 and 1 protocols). This is not a surprise, as current standards and technology aim for *short* range, high bit-rate per tag applications and not the opposite (extended range, low bit-rate).

Moreover, in cases where there is no receiver structure at

each sensor, the utilization of tree-based/CSMA anti-collision becomes impossible. An alternative solution is the use of time-domain spread spectrum techniques at the physical layer [8]. For the case of backscatter sensor networks in [4], [5], the modulating (subcarrier) frequency at each sensor was assumed *sufficiently* different from all the rest, keeping interference among simultaneously operating sensors minimal.

In this work, we build upon the idea of ultra low-cost backscatter sensor networks and attempt to analyze, mathematically quantify and alleviate the collision problem among a large number of simultaneously operating, low bit-rate, receiver-less sensors based on backscatter communication, i.e. backscatter sensor networks (BSNs).

Specifically, this work:

1) Discovers that anti-collision performance in high-density BSNs is feasible provided that appropriate modulation is used at each sensor. Specifically, it shown that a broad class of tag modulations, typically found in short-range scenarios, require prohibitively large aggregate bandwidth for acceptable anti-collision performance. That is due to the round-trip nature of backscatter communication as well as the extended target range, which both impose stringent requirements on spectrum efficiency, not easily met by all modulations.
2) Provides general, closed-form analysis that quantifies sensor collision (interference) in high-density, backscatter sensor networks (BSN), as a function of number of tags and aggregate bandwidth. Analysis is applicable to a broad class of sensor subcarrier modulations, propagation environments and reader antenna directivity patterns.
3) Quantifies aggregate bandwidth savings for given anti-collision performance when simple division techniques on subcarrier (modulating) frequency and space (via moderately directive hub antenna) are combined. Emphasis is given on large number of sensors operating over backscatter, which is radically different that conventional (one-way) radio.

Bandwidth reduction and network scalability become crucial in backscatter radio systems; allocated industrial scientific and medical (ISM) bands around the world offer limited and variable frequencies, e.g. UHF ISM bands in U.S. provide $\sim$ 26 MHz bandwidth ($902-928$ MHz) while European UHF ISM bands provide only ~ 3 MHz ($865-868$ MHz). Similar limited UHF bandwidth is also observed in Asia (on the order of a few MHz). Thus, efforts to solve the bandwidth scarcity and scalability problem could potentially assist successful adoption of backscatter radio systems worldwide. It is noted that worldwide adoption of RFID standards is currently considered one of the major industry *business risks* [9].

Section II provides the system model and the basic assumptions behind this work, section III presents the analytical results for three cases of hub (reader) antenna, section IV provides analysis extensions including tag clustering and reader collision and section V offers the numerical results. Finally, conclusion is provided in section VI.

II. System Model

$N+1$ sensors (tags) are placed randomly and independently around the hub (reader), with the objective to monitor a geographical area of radius in $[d_{\min}, d_{\max}]$ (Fig. 1). All ranges in that interval are equally important in terms of the sensing objective, and therefore, the range d_i of sensor $i \in \{0, 1, \ldots, N\}$ is assumed uniform in the above interval. Similarly, the bearing angle ϕ_i of each sensor is assumed uniform in $[0, 2\pi]$. In section IV-A, we relax the latter assumption and allow a subset of sensors to be clustered within an angular section.

Similarly to [4], each sensor alternates the antenna impedance between two states, utilizing a simple RF transistor switch. In that way, binary modulation of the reflected carrier is possible, even though the sensor does not actively transmits any radio signal. The backscattered signal is picked by the hub and processed to extract the modulated information. Note that for each tag i two frequencies are involved: the frequency of the carrier f_c transmitted from the hub (common for all tags and on the order of MHz or GHz), and the subcarrier frequency of that tag f_{si}, which is the frequency of alternation between two switch states (on the order of Hz or KHz depending on the required low bit-rate).

The modulation of that subcarrier frequency carries the transmitted message from a specific tag, and subcarrier frequency separation δ is assumed, amounting to aggregate communication bandwidth proportional to $(N+1)\delta$. Each tag has a unique subcarrier frequency, allocated randomly (i.e. not carefully), based on the uniform distribution among $N+1$ available subcarrier frequencies. Such allocation in practice requires that each sensor (tag) has a known and unique ID (which is reasonable to assume even for large N). Fig. 2 depicts this scenario for BFSK modulation implemented at each sensor.

The *average* received (at the hub) power p_i of the signal backscattered by tag i is described by:

$$p_i(d_i, \phi_i) = \eta \; L_i^2 \; P_{\mathrm{H}}, \tag{1}$$

where P_{H} is the hub transmitted power, L_i is the one-way propagation loss and η is the *backscattering* efficiency of the tag antenna, assuming that all tag antennas are the same. Efficiency η depends on the tag antenna aperture and the *differential* radar cross section (RCS), which in turn depends on the termination loads, alternatively connected to the tag antenna during subcarrier modulation [10], [11]. For passive tags, the designer aims to maximize both power transfer towards the tag circuitry as well as power scattered back to the hub. Therefore, both choice of subcarrier modulation as well as relevant duty cycle affect *powering* of passive tags, in contrast to backscatter sensor networks where battery is already available at each tag to power sensor electronics.

Note that propagation loss is squared, due to the round-trip nature of backscatter communication, as opposed to conventional one-way radio propagation. One-way propagation loss L_i can be given by the familiar (free space) Friis equation:

$$L_i = \; G_{\mathrm{S}} \; G_{\mathrm{H}}(\phi_i) \; \left(\frac{\lambda}{4\pi d_i}\right)^2, \tag{2}$$

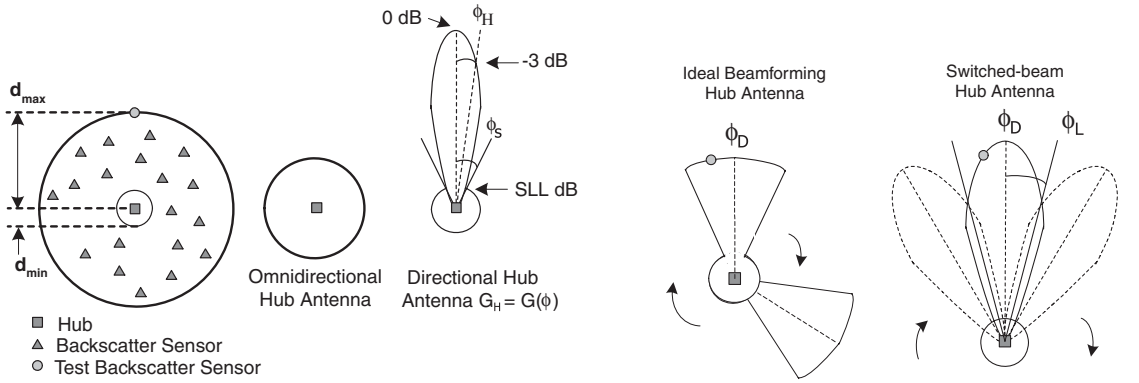

(a) Network.

(b) Ideal and switched-beam (non-ideal) beamforming hub antenna.

Fig. 1. Network setup for a single hub (reader). Three cases of reader antenna are considered.

where $G_{\rm S}$ is the gain of the sensor antenna (assuming appropriate alignment for all tags), $G_{\rm H}(\phi_i)$ is the gain of the hub antenna at the direction ϕ_i of tag i, and λ is the wavelength of the carrier. For scenarios different than the free-space above, power drops faster with distance and various approximations can be used, dependent on the wireless environment. For example, when $d_i \geq d_{\rm th}$, with

$$d_{\rm th} = \frac{4\pi h_{\rm H} h_{\rm S}}{\lambda}, \tag{3}$$

and $h_{\rm H}, h_{\rm S}$ the hub and tag antenna heights respectively, one way loss can be approximated by [12]:

$$L_i = \; G_{\rm S}\; G_{\rm H}(\phi_i)\; \left(\frac{h_{\rm H} h_{\rm S}}{{d_i}^2}\right)^2, \text{ if } d_i \geq \frac{4\pi h_{\rm H} h_{\rm S}}{\lambda}, \tag{4}$$

while the Friis formula can be used for $d_i < \frac{4\pi h_{\rm H} h_{\rm S}}{\lambda}$. Accordingly, a general two-slope model for one way propagation loss is adopted in this work:

$$L_i = \begin{cases} G_{\rm S}\; G_{\rm H}(\phi_i)\; \chi_1\; (1/d_i^{A_1}), & \text{if } d_i < d_{\rm th} \\ G_{\rm S}\; G_{\rm H}(\phi_i)\; \chi_2\; (1/d_i^{A_2}), & \text{if } d_i \geq d_{\rm th} \end{cases} \tag{5}$$

with $0 \leq A_1 < A_2$ and all involved quantities above being positive. Within this model, average power loss is not necessarily restricted to an integer power of distance but instead can be expanded to more general cases, typically found in measuring campaigns (e.g. [13] measures and estimates $A_1 = 2.04$ up to 11 meters and $A_2 = 7.4$ above).

For the case of an omni hub antenna, $G_{\rm H}(\phi_i)$ is simplified to $G_{\rm H}(\phi_i) = 1$. For the case of beamforming at the hub antenna, the pattern is expressed as:

$$G_{\rm H}(\phi_i) = \begin{cases} G_0(\phi_i - \phi_D), & \phi_D - \phi_S \leq \phi_i \leq \phi_D + \phi_S, \\ G_0^{\max}\; 10^{\mathsf{SLL}/10} = a_0 G_0^{\max}, & \text{elsewhere}, \end{cases} \tag{6}$$

where $G_0(\phi)$ describes the main lobe as function of angle and ϕ_D is the direction of hub antenna observation, corresponding to the main beam maximum $G_0(\phi_D) \stackrel{\triangle}{=} \max\{G_0(\phi)\} \equiv G_0^{\max}$. Without loss of generality, we assume a symmetric main lobe around the direction of observation ($G_0(\phi_D - \phi) = G_0(\phi_D + \phi)$), without any other restrictions on its shape (Fig. 1).[1] Furthermore, SLL denotes the antenna side lobe level in dB and $2\phi_S$ describes the beamwidth of the antenna up to the SLL level. For a practical switched-beam hub antenna, the rotation of the beam occurs in predetermined steps and thus, specific overlap angle ϕ_L between two consecutive, neighboring in space, beams (Fig. 1).

In contrast, an ideal beamforming hub antenna assumes that main lobe readouts occur with maximum (and constant) gain $G_0^{\max}$ for $\phi_D - \phi_S \leq \phi_i \leq \phi_D + \phi_S$. This corresponds to the ideal case where the hub antenna can switch the main beam with maximum spatial resolution and thus, "illuminate" the tag of interest with maximum antenna gain. It is further assumed that the beamforming antenna scans the whole area (i.e. $\phi_D \in [0, 2\pi]$), with such speed that allows the appropriate number of reads per sensor per second.

It is noted that according to the above model, interfering tags (sensors) outside the main lobe are attenuated according to SLL, even though in practice the attenuation will be even greater, according to the specifics of the antenna pattern. Therefore, the antenna model provides worst-case collision analysis results, while it is general enough to encompass a broad class of reader antenna designs: only the values of SLL, ϕ_S (for ideal beamforming) and additionally ϕ_L and $G_0(\phi_D - \phi_L)$ (for switched-beam antenna) are needed, without requiring any further knowledge of the antenna pattern. The specific values used for the numerical results section are taken from well-understood antenna designs found in the literature, with moderate side lobe levels and main lobe widths.

Consecutively, the signal-to-interference-noise ratio SINR for each tag i is expressed as:

$$\mathsf{SINR}_i \;\; = \;\; \frac{\frac{1}{R}\; g_i\; p_i}{\frac{1}{R}\; \sum_{j \neq i} s_{ij}\; g_j\; p_j + \mathcal{N}_0}, \tag{7}$$

where $\mathcal{N}_0$ is the average noise power spectral density (Watt/Hz) at the hub,[2] R is the bit-rate of each tag and g_i is an exponential random variable with $\mathbb{E}\{g_i\} = 1$, corresponding to Rayleigh fading for the round-trip channel path between hub and tag i. It is further assumed that small-scale fading $\{g_j\}$ is

[1] A non-symmetric main lobe around the direction of observation could imply design or manufacturing error.

[2] including thermal noise, as well as receiver noise figure NF at the hub.

independent across the various distributed tags. Such fading model emerges when channel is affected by many independent parameters in difficult propagation environments without line-of-sight, providing reference, worst-case analysis results. Note that due to the low-bit rate of each sensor and the corresponding extended duration of each information bit considered in this work (on the order of hundreds of milliseconds), channel fluctuations may happen within a single or a few consecutive bits. Therefore, predicting all parameters that affect channel fluctuations and employing a different fading model for the low-bit rate backscatter channel with range of several tens of meters, set another research challenge, beyond the scope of this paper. Attempts to model the backscatter radio channel already exist: work in [14] experimentally studies fading in indoor, limited-range (up to approximately 10 meters from the hub) environments, while work in [15] models backscatter radio channel fading as a product of Rayleigh random variables with varying degree of correlation and bi-static reader (i.e. reader with distinct transmit and receive antennas).

The parameter s_{ij} is inversely proportional to the subcarrier frequency separation between tag i and tag j. It depends on the spectral efficiency of the specific binary modulation implemented at each tag and the filtering functions at the hub:

$$s_{ij} = \kappa^{-\nu} |f_{\mathrm{s}i} - f_{\mathrm{s}j}|^{-\nu}. \tag{8}$$

For ASK or BPSK modulation, $\nu = 2$, while for MSK modulation, $\nu = 4$. Specifically, it can be shown that for BPSK modulation, the power spectrum drops for large frequencies f with $1/(2\pi f/R)^2$ ($\kappa = 2\pi/R$), while for MSK the power spectrum drops much faster with $1/(5f/R)^4$ ($\kappa = 5/R$) [16]. The latter modulation is a special case of BFSK, with continuous phase transition between consecutive symbols (bits) and as such, power spectrum drops faster than non-continuous phase counterparts (e.g. BPSK, general BFSK). Implementing MSK modulation at each sensor is feasible with low-cost, phase-locked loops (PLL).

Finally, it is noted that the signal-to-noise-and-interference expression of Eq. (7) is general enough to accommodate immobile sensors or sensors with reduced mobility (i.e. mobility that amounts to Doppler shift smaller than the required bandwidth per sensor). However, the latter case requires non-trivial detection techniques robust to mobility, especially when Doppler shift becomes comparable to the subcarrier (modulating) frequency spacing δ between sensors. Detection techniques are beyond the scope of this work and relevant examples for the low-bit rate, extended-range backscatter radio channel employed in this work can be found in [4], [5].

III. Collision Analysis

Given that each tag operates on different subcarrier frequency, interference to any tag is caused by tags that operate in neighboring subcarrier frequencies (Fig. 2). By using a directive hub antenna instead of an omni antenna, interference is limited to tags that are close in subcarrier frequency *and* (geographic) space. Outage probability for a test sensor at the edge of coverage is the performance criterion. Without loss of generality, we assume that the test sensor 0 is located at $d_0 = d_{\max}$. The outage event $\mathsf{SINR}_0 < \Theta$ occurs when

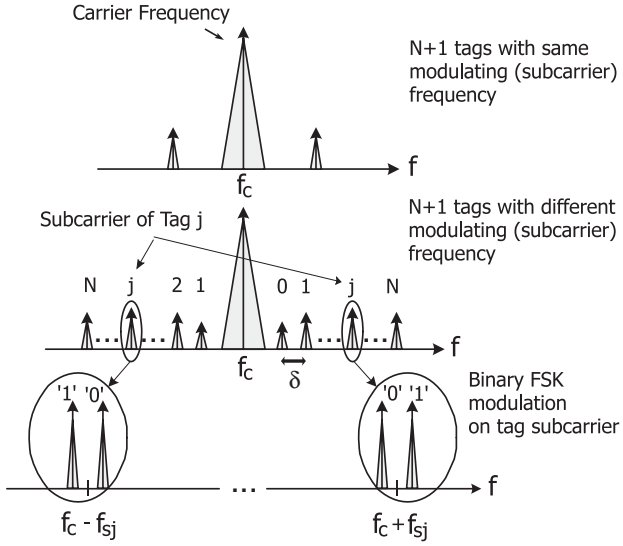

Fig. 2. $N+1$ sensors (tags) binary-modulate information on a subcarrier frequency, i.e. the frequency of switching a transistor between two states. The specific case of BFSK modulation at each sensor is depicted.

the SINR for the test sensor drops below a predetermined threshold Θ, necessary for detection at the hub receiver. Notice that received power p_0 (and consecutively outage probability) for a practical (non-ideal) hub antenna depends on the test tag angle ϕ_0, while it is independent on ϕ_0 for ideal hub beamformer (as described above) or for omni hub antenna:

$$\begin{aligned}\mathbb{P}_{\mathrm{out}|\phi_0} &\triangleq \mathbb{P}\left\{\mathsf{SINR}_0 < \Theta \mid \phi_0\right\} \\ &= \Pr\left(g_0 < \frac{R\ \Theta\ \mathcal{N}_0}{p_0} + \frac{\Theta}{p_0}\sum_{j=1}^{N} s_{0j}\ g_j\ p_j\right) \qquad (9) \\ &= 1 - e^{\left(-\frac{R\ \Theta\ \mathcal{N}_0}{p_0}\right)}\ \mathbb{E}\left\{\prod_{j=1}^{N}\frac{1}{1+\Theta\ s_{0j}\ \frac{p_j}{p_0}}\right\}, \qquad (10)\end{aligned}$$

where we have used the fact that the random variables $\{g_i\}_{i=0}^{N}$ are independent and independent of $\{s_{0i}\}_{i=1}^{N}$ and $\{p_i\}_{i=1}^{N}$.

On the other hand, the random variables $\{s_{0i}\}_{i=1}^{N}$ are identically distributed but not independent in the general case. Let $s_{0i} = \kappa^{-\nu}|f_{\mathrm{s}0} - f_{\mathrm{s}i}|^{-\nu}$ and $s_{0j} = \kappa^{-\nu}|f_{\mathrm{s}0} - f_{\mathrm{s}j}|^{-\nu}$ with $i \neq j, \forall\ i,j\ \in\ \{1,2,\ldots,N\}$. The two identically distributed random variables require $f_{\mathrm{s}i} \neq f_{\mathrm{s}j}$ due to the uniform permutation of N available frequencies for N interfering sensors to the test tag. Therefore, for any $i \neq j, \forall\ i,j\ \in\ \{1,2,\ldots,N\}$ there is dependence between s_{0j} and s_{0i}. However, that dependence is strictly due to the above inequality constraint $f_{\mathrm{s}j} \neq f_{\mathrm{s}i}$ and can be relaxed (i.e. the random variables can be considered independent) for large N. Consider the following identically distributed random variables $\{S_j\}_{j=1}^{N}$, with S_j given by:

$$S_j = \kappa^{-\nu}|f_{\mathrm{s}0} - f_{\mathrm{s}}|^{-\nu} \tag{11}$$

$$= \begin{cases} \kappa^{-\nu}|f_{\mathrm{s}0} - f_{\mathrm{s}j}|^{-\nu}, \\ \text{or} \\ \kappa^{-\nu}|f_{\mathrm{s}0} - f_{\mathrm{s}i}|^{-\nu}, \quad i \neq j,\ i \in \{1,2,\ldots,N\}, \end{cases} \tag{12}$$

where $f_{\mathrm{s}} \neq f_{\mathrm{s}0}$. That is a random variable that involves *all* N available subcarrier frequencies $\{f_{\mathrm{s}j}\}_{j=1}^{N}$, i.e. the value of S_j does not depend on the value of S_i, for any $i \neq j$. In other

words, the restriction $f_{\rm sj} \neq f_{\rm si}$ does not exist and the identically distributed random variables $\{S_j\}_{j=1}^N$ are independent. The lower branch of S_j corresponds to the random variable s_{0i} and it can be seen that $S_j \equiv s_{0i}$ with probability $(N-1)/N$, according to Eq. (12). Therefore, for $\frac{N-1}{N} \to 1$, or equivalently for large N, the identically distributed random variables $\{s_{0i}\}_{i=1}^N$ can be considered independent. The numerical results presented later for N on the order of 100 or greater, further validate the above.

The purpose of this work is to evaluate anti-collision performance for large number of sensors. Thus, assuming large N (or equivalently $\frac{N-1}{N} \to 1$) and exploiting the fact that the random variables $\{p_j\}_{j=1}^N$ are independent and identically distributed, Eq. (10) is further simplified:

$$\mathbb{P}_{\text{out}|\phi_0} \to 1 - e^{\left(-\frac{R \ \Theta \ \mathcal{N}_0}{p_0}\right)\mathsf{Y}^N},$$
$$\mathsf{Y} = \mathbb{E}\left\{\frac{1}{1+\Theta \ s_{0j} \ \frac{p_j}{p_0}} \ |\phi_0\right\}, \frac{N-1}{N} \to 1. \tag{13}$$

Notice that interference to the test tag from the rest of the sensors (a.k.a. *collision*) is restricted to the term $0 < \mathsf{Y} \leq 1$. The collision parameter Y is further simplified for the three cases of hub antenna below, assuming $d_{\min} < d_{\text{th}} < d_{\max}$.

A. Omni Hub Antenna:

For omnidirectional hub antenna $G_{\rm H} = 1$. We first need to calculate the statistics of the identically distributed random variables $\{s_{0j}\}_{j=1}^N$. Notice that the $N+1$ subcarrier (modulating) frequencies $\{f_{\rm sj}\}_0^N$ are unique (different), equally spaced every δ and they are distributed according to a uniform permutation. Consecutively, the following expressions hold:

$$\{s_{0j}\}_{j=1}^N = \kappa^{-\nu}|f_{\rm s0} - f_{\rm sj}|^{-\nu} \tag{14}$$
$$= \kappa^{-\nu}\mu^{-\nu}\delta^{-\nu}, \quad \mu \in \{1,2,\ldots,N\}, \tag{15}$$

and

$$\Pr(\mu) = \frac{2(N+1-\mu)}{N(N+1)}, \quad \mu \in \{1,2,\ldots,N\}. \tag{16}$$

The term 2 above is due to the absolute value in Eq. (14), the term $\frac{1}{N(N+1)}$ is due to the fact that $f_{\rm s0}$ and $f_{\rm sj}, (\ j \neq 0)$, are uniformly selected among $N+1$ and N different frequencies respectively, while the term $(N+1-\mu)$ denotes the number of all frequency pairs where the two frequencies (among $N+1$ candidates) are spaced exactly by $\mu\delta$.

Combining Eqs. (13), (16), we get:

$$\mathsf{Y} = \mathbb{E}\left\{\frac{1}{1+\Theta \ s_{0j} \ \frac{p_j}{p_0}} \ |\phi_0\right\}$$
$$= \sum_{\mu=1}^{N} \frac{2(N+1-\mu)}{N(N+1)} \int_{d_{\min}}^{d_{\max}} \frac{1}{1+\Theta \ \kappa^{-\nu} \ \mu^{-\nu} \ \delta^{-\nu} \ \frac{p_j}{p_0}} \ dp_j \tag{17}$$

$$= \frac{1}{d_{\max} - d_{\min}} \sum_{\mu=1}^{N} \frac{2(N+1-\mu)}{N(N+1)} \times$$
$$\times \Big[g_1(d_{\text{th}}, \Theta_1(\mu), 2A_1) - g_1(d_{\min}, \Theta_1(\mu), 2A_1) +$$
$$+ \ g_1(d_{\max}, \Theta_2(\mu), 2A_2) - g_1(d_{\text{th}}, \Theta_2(\mu), 2A_2)\Big], \tag{18}$$

where

$$\begin{cases} \Theta_1(\mu) & = \Theta \ \kappa^{-\nu}\mu^{-\nu}\delta^{-\nu} \ \left(\frac{\chi_1}{\chi_2}\right)^2 \ d_{\max}^{2A_2}, \\ \Theta_2(\mu) & = \Theta \ \kappa^{-\nu}\mu^{-\nu}\delta^{-\nu} \ d_{\max}^{2A_2}, \end{cases} \tag{19}$$

and

$$g_1(y;\Theta,2A) = \int \frac{1}{1+\Theta \ y^{-2A}} \ dy \tag{20}$$
$$= \begin{cases} y - y \ {}_2F_1\left(\frac{1}{2A}, 1; 1+\frac{1}{2A}; -\frac{y^{2A}}{\Theta}\right), & |\Theta \ y^{-2A}| > 1, \\ y \ {}_2F_1\left(-\frac{1}{2A}, 1; 1-\frac{1}{2A}; -\frac{\Theta}{y^{2A}}\right), & |\Theta \ y^{-2A}| < 1, \\ \frac{y}{2}, & \Theta \ y^{-2A} = 1. \end{cases}$$

It is noted that ${}_2F_1\,(a,b;c;z)$ is the Gauss hypergeometric function [17], which is implemented in most computation software packages or can be evaluated numerically. The proof of Eq. (20) is given at the appendix. For the special case of $A = 2$ or $A = 4$, Eq. (20) can be further simplified to expressions with elementary trigonometric functions. The above expressions however are applicable for *any* propagation environment (estimated or measured in practice), where A_1, A_2 are not necessarily integers.

As expected, it can be seen from the above that for omni hub antenna, the edge outage probability is independent of ϕ_0 and thus,

$$\mathbb{P}_{\text{out}}^{\text{omni}} \equiv \mathbb{P}_{\text{out}|\phi_0}. \tag{21}$$

Furthermore, a sufficient condition for collision-free performance $\mathsf{Y} \simeq 1$ can be derived by examining the denominator at the integral of Eq. (17). Given that $A_1 < A_2$ and $d_{\min} < d_{\text{th}}$ and assuming $d_{\text{th}}^{-2A_2} < \left(\frac{\chi_1}{\chi_2}\right)^2 \ d_{\min}^{-2A_1}$, it can be seen that:

$$\Theta \ \kappa^{-\nu}\mu^{-\nu}\delta^{-\nu}\frac{p_j}{p_0} < \Theta \ \frac{\chi_1^2}{\chi_2^2}\kappa^{-\nu}\delta^{-\nu}\left(\frac{d_{\max}^{A_2}}{d_{\min}^{A_1}}\right)^2, \forall \ \mu. \tag{22}$$

By setting the above upper bound much less than unity, the denominator of Eq. (17) approaches unity:

$$\delta_0 \triangleq \left[\Theta \ \frac{\chi_1^2}{\chi_2^2} \ \frac{1}{\kappa^\nu} \ \left(\frac{d_{\max}^{A_2}}{d_{\min}^{A_1}}\right)^2\right]^{1/\nu} << \delta \tag{23}$$
$$\Rightarrow \Theta \ \kappa^{-\nu}\mu^{-\nu}\delta^{-\nu}\frac{p_j}{p_0} << 1$$
$$\Rightarrow 1 + \Theta \ \kappa^{-\nu}\mu^{-\nu}\delta^{-\nu}\frac{p_j}{p_0} \to 1$$
$$\Rightarrow \mathsf{Y} \to 1, \tag{24}$$

or equivalently:

$$\delta_0 << \delta \Rightarrow 1 + \frac{\delta_0}{\delta} \to 1 \Rightarrow \mathsf{Y} \to 1. \tag{25}$$

Notice in Eq. (23) that the ratio between smaller and larger distances raised to the appropriate path loss exponent, is raised to the second power, exactly due to the round trip nature of backscatter communication. That implies that the ratio between the stronger and the weakest signal, i.e. the expected *dynamic range* in BSNs, is significantly larger than in systems operating by means of conventional one-way radio.

The above sufficient condition for collision-free performance provides a quick way to calculate sufficient spacing δ between modulating (subcarrier) frequencies (e.g. $\delta \simeq 10\delta_0$)

that offers robust anti-collision performance. It will be seen in the numerical results section that even $\delta = 5\delta_0$ provides acceptable anti-collision performance, with omnidirectional hub antenna. Consecutively, estimation of the aggregate bandwidth per reader (proportional to $(N+1)\delta$) for a given number of tags can be performed.

B. Ideal Beamforming Hub Antenna:

The ideal beamforming hub antenna "illuminates" the test sensor with maximum gain. Thus, $G_{\mathrm{H}}(\phi_0) = G_0^{\max}$ and for any other sensor, $G_{\mathrm{H}}(\phi_i) = G_0^{\max}$, if sensor i is inside the antenna main lobe, and $G_{\mathrm{H}}(\phi_i) = G_0^{\max} 10^{\mathsf{SLL}/10} = a_0 G_0^{\max}$, when interfering sensor i is located outside the antenna main lobe (sector). Given that ϕ_i is uniformly distributed, the interfering term Y becomes:

$$\mathsf{Y} = \frac{\phi_S}{\pi}\,\mathbb{E}\left\{\frac{1}{1+\Theta\ s_{0j}\ \frac{p_j}{p_0}}\middle|\ G_{\mathrm{H}}(\phi_j) \to 0\ \mathrm{dB}\right\} + \\ + \frac{\pi-\phi_S}{\pi}\ \mathbb{E}\left\{\frac{1}{1+\Theta\ s_{0j}\ \frac{p_j}{p_0}}\middle|\ G_{\mathrm{H}}(\phi_j) \to \mathsf{SLL}\ \mathrm{dB}\right\}. \quad (26)$$

The first expected value above has already been calculated in subsection III-A for omni hub antenna. The second expected value can be readily calculated from the same expressions with $a_0^2\Theta$ instead of Θ.

For (ideal) beamforming hub antenna, as described before, the edge outage probability for the test sensor is independent of ϕ_0 and thus,

$$\mathbb{P}_{\mathrm{out}}^{\mathrm{ideal}} \equiv \mathbb{P}_{\mathrm{out}|\phi_0}. \quad (27)$$

C. Switched-Beam Hub Antenna:

For the case of switched-beam hub antenna, the test tag may not be "illuminated" with maximum gain, given that practical antenna designs switch the main lobe in discrete steps (Fig. 1). At the worst case in terms of performance, the tag is "illuminated" with minimum antenna gain $G_{\mathrm{H}}(\phi_D - \phi_L)$, while the interfering tags with maximum gain $G_0^{\max}$:

$$\mathbb{P}_{\mathrm{out}}^{\mathrm{switch}} \le \left\{1 - e^{\left(-\frac{R\ \Theta\ \mathcal{N}_0}{p_0}\right)}\mathsf{Y}^N\ \middle|\phi_0 = \phi_L\right\} \\ \le \left\{1 - e^{\left(-\frac{R\ \Theta\ \mathcal{N}_0}{p_0}\right)}\mathsf{Y_L}^N\ \middle|\phi_0 = \phi_L\right\}, \quad (28)$$

where

$$\mathsf{Y} \ge \mathsf{Y_L} = \frac{\phi_S}{\pi}\,\mathbb{E}\left\{\frac{1}{1+\Theta\ s_{0j}\ \frac{p_j}{p_0}}\middle|\ G_{\mathrm{H}}(\phi_j) \to 0\ \mathrm{dB}\right\} + \\ + \frac{\pi-\phi_S}{\pi}\ \mathbb{E}\left\{\frac{1}{1+\Theta\ s_{0j}\ \frac{p_j}{p_0}}\middle|\ G_{\mathrm{H}}(\phi_j) \to \mathsf{SLL}\ \mathrm{dB}\right\}. \quad (29)$$

At the above expression, p_0 is calculated at ϕ_L ($G_{\mathrm{H}}(\phi_0) = G_0(\phi_D - \phi_L)$). Moreover, the first expected value in (29) is calculated using the expressions of subsection III-A, with $\Theta\left(\frac{G_0^{\max}}{G_0(\phi_L-\phi_D)}\right)^2$ instead of Θ. Similarly, the second expected value is calculated with $\Theta\left(\frac{G_0^{\max}\ a_0}{G_0(\phi_L-\phi_D)}\right)^2$ instead of Θ.

On the contrary, the best case in terms of performance, occurs when the test tag is "illuminated" with maximum hub antenna gain ($\phi_0 = \phi_D$), while all interfering tags are outside the main lobe of the antenna:

$$\mathbb{P}_{\mathrm{out}}^{\mathrm{switch}} \ge \left\{1 - e^{\left(-\frac{R\ \Theta\ \mathcal{N}_0}{p_0}\right)}\mathsf{Y}^N\ \middle|\phi_0 = \phi_D\right\} \\ \ge \left\{1 - e^{\left(-\frac{R\ \Theta\ \mathcal{N}_0}{p_0}\right)}\mathsf{Y_U}^N\ \middle|\phi_0 = \phi_D\right\}, \quad (30)$$

where

$$\mathsf{Y} \le \mathsf{Y_U} = \mathbb{E}\left\{\frac{1}{1+\Theta\ s_{0j}\ \frac{p_j}{p_0}}\middle|\ G_{\mathrm{H}}(\phi_j) \to \mathsf{SLL}\ \mathrm{dB}\right\}. \quad (31)$$

At the above expression, p_0 is calculated at ϕ_D ($G_{\mathrm{H}}(\phi_0) = G_0^{\max}$). Moreover, the expected value in (31) is calculated using the expressions of subsection III-A, with $a_0^2\ \Theta$ instead of Θ.

Notice that both lower and upper performance bounds above can be calculated in closed-form, for *any* antenna gain pattern, symmetric around observation direction ϕ_D (Fig. 1).

IV. Analysis Extensions

A. Non-identical Sensors

Assuming large N (or equivalently $\frac{N-1}{N} \to 1$) and independent but not identically distributed sensors, Eq. (10) is simplified to:

$$\mathbb{P}_{\mathrm{out}|\phi_0} = 1 - e^{\left(-\frac{R\ \Theta\ \mathcal{N}_0}{p_0}\right)} \times \\ \times \prod_{j=1}^{N}\mathbb{E}\left\{\frac{1}{1+\Theta\ s_{0j}\ \frac{p_j}{p_0}}\ |\phi_0\right\},\ \frac{N-1}{N} \to 1. \quad (32)$$

The above formula can be used to calculate performance for the general case of sensors distributed independently, in any random way.

Consider for example the case of total $N = N_1 + N_2$ sensors, where N_1 sensors are uniformly distributed as before (set $\{N_1\}$) and N_2 sensors are clustered within a section of angular width $2\phi_{\mathrm{N2}}$ (Fig. 3) and $\{d_j\}$ independent, uniformly distributed in $[d_{\mathrm{min2}}, d_{\mathrm{max2}}]$ (set $\{N_2\}$). We further assume cluster angular width $\phi_{\mathrm{N2}} > \phi_{\mathrm{S}}$ and $d_{\mathrm{min2}} < d_{\mathrm{th}} < d_{\mathrm{max2}}$. Accordingly, Eq. (33) is further simplified to:

$$\mathbb{P}_{\mathrm{out}|\phi_0} = 1 - e^{\left(-\frac{R\ \Theta\ \mathcal{N}_0}{p_0}\right)}\ \mathsf{Y}_1^{N_1}\ \mathsf{Y}_2^{N_2}, \\ \mathsf{Y}_1 = \mathbb{E}\left\{\frac{1}{1+\Theta\ s_{0i}\ \frac{p_i}{p_0}}\ |\phi_0, i \in \{N_1\}\right\}, \\ \mathsf{Y}_2 = \mathbb{E}\left\{\frac{1}{1+\Theta\ s_{0j}\ \frac{p_j}{p_0}}\ |\phi_0, j \in \{N_2\}\right\}. \quad (33)$$

For the case of omnidirectional hub antenna, Y_1 is readily given by Eqs. (18),(19),(20), while Y_2 is calculated from the same formulas after substituting $d_{\mathrm{min2}} \to d_{\mathrm{min}}$ and $d_{\mathrm{max2}} \to d_{\mathrm{max}}$. For the case of ideal beamforming hub antenna, Y_1 is calculated according to Eq. (26), while calculation of Y_2 assumes the worst case scenario, where most interfering tags in $\{N_2\}$ are clustered within the antenna observation sector. Assuming observation direction $\phi_{\mathrm{D}} = \phi_0$, such scenario occurs with $|\phi_j - \phi_{\mathrm{D}}| < \phi_{\mathrm{N2}}\ \forall\ j \in \{N_2\}$. For uniform

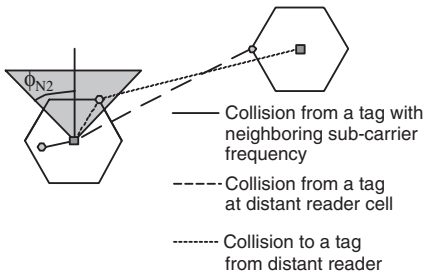

Fig. 3. Intra-cell interference is caused by tags at the same cell with neighboring modulating (subcarrier) frequency. Inter-cell interference is caused by tags and readers with same subcarrier and carrier frequencies respectively at distant cells.

distribution of ϕ_j in $[\phi_{\rm D}-\phi_{\rm N2}, \phi_{\rm D}+\phi_{\rm N2}]$, Y_2 is calculated by:

$$\mathsf{Y}_2 = \frac{\phi_S}{\phi_{\rm N2}}\,\mathbb{E}\left\{\frac{1}{1+\Theta\ s_{0j}\ \frac{p_j}{p_0}}\,\middle|\ G_{\rm H}(\phi_j)\to 0\ \text{dB}\right\} + \\ + \frac{\phi_{\rm N2}-\phi_S}{\phi_{\rm N2}}\ \mathbb{E}\left\{\frac{1}{1+\Theta\ s_{0j}\ \frac{p_j}{p_0}}\,\middle|\ G_{\rm H}(\phi_j)\to \mathsf{SLL}\ \text{dB}\right\}. \tag{34}$$

The first expected value is calculated according to subsection III-A for omni hub antenna (after substituting $d_{\rm min2}\to d_{\rm min}$ and $d_{\rm max2}\to d_{\rm max}$) and the second expected value is calculated from the same expressions with $a_0^2\Theta$ instead of Θ. As described before, the edge outage probability for the test sensor is independent of ϕ_0 for omni or ideal beamforming antenna and thus, $\mathbb{P}_{\rm out}\equiv\mathbb{P}_{{\rm out}|\phi_0}$.

B. Collision from Other Reader Cells

Up to now, we have calculated the collision probability due to tags that belong to the *same* cell, covered by a specific reader (hub). The use of directive reader antenna per cell restricts sources of collision and therefore reduces collision probability compared to scenarios with omnidirectional reader antenna. Equivalently, for *given* target collision probability and number of tags, the use of a directive antenna at the hub decreases the modulating frequency spacing δ among the tags compared to networks with omnidirectional antenna for each reader. This is important since bandwidth reduction per reader (due to directive antennas) is translated to better frequency reuse (higher frequency reuse factor) and smaller interference caused by *distant* tags and readers that operate on the same frequencies (Fig. 3).

Specifically, if $W_{\rm c}\propto(N+1)\delta$ is the amount of bandwidth per cell, then the total bandwidth required to cover an extended geographical area with multiple readers becomes $W_{\rm tot}=K\ W_{\rm c}$, where K is the frequency reuse factor. Therefore, any value δ for modulating frequency separation among the sensors corresponds to a specific value of frequency reuse K across the network:

$$\mathbb{P}_{\rm out}=\text{const}, W_{\rm tot}=\text{const}\Rightarrow \\ K_{\rm omni}(N+1)\delta_{\rm omni}=K_{\rm beam}(N+1)\delta_{\rm beam}. \tag{35}$$

If we manage to decrease subcarrier frequency separation from $\delta_{\rm omni}$ to $\delta_{\rm beam}$ $(\delta_{\rm beam}<\delta_{\rm omni})$ for a given number of tags $N+1$, given target collision probability $\mathbb{P}_{\rm out}$ and aggregate bandwidth $W_{\rm tot}$, we consecutively increase the frequency reuse factor K $(K_{\rm beam}>K_{\rm omni})$ and the effective reuse distance D between same frequency (in-band) readers. The latter decreases reader collision, as well as tag collision from a tag that operates on same modulating (*subcarrier*) frequency at a distant reader cell (Fig. 3).

Accordingly, when a single tier of same-subcarrier frequency interfering readers at hexagonal cells of radius $\mathcal{R}$ is considered, the reuse distance becomes $D=\mathcal{R}\sqrt{3K}$ and the signal-to-interference ratio at a given reader due to interference from a distant tag i.e. a tag that operates on the same subcarrier frequency and belongs to a different reader cell (Fig. 3), can be expressed as:

$$\frac{\rm S}{\rm I_{tag}}\simeq\frac{\mathcal{R}^{-2A_2}}{6D^{-2A_2}}=\frac{1}{6\left(\sqrt{3K}\right)^{-2A_2}}, \tag{36}$$

where A_2 is the one-way propagation loss exponent, defined before and the term $2A_2$ considers the two-way, round-trip nature of backscatter communication. Combining Eqs. (35), (36), it is found that any decrease of modulating (tag) frequency from $\delta_{\rm omni}$ to $\delta_{\rm beam}$ $(\delta_{\rm beam}<\delta_{\rm omni})$, reduces the interference from other cell tags of same modulating frequency by the following factor (in dB):

$$\left(\frac{\rm S}{\rm I_{tag}}\right)_{\rm gain}=10\log_{10}\left[\left(\sqrt{\frac{\delta_{\rm omni}}{\delta_{\rm beam}}}\right)^{2A_2}\right]. \tag{37}$$

Notice that the reduction of δ doubles the gain (in dB) compared to conventional radio, due to the round trip nature of backscatter communication.

Similarly, the signal-to-interference ratio at a given reader due to interference from the carrier transmitted by a distant reader i.e. a reader that operates on the same *carrier* frequency covering a distant geographical region (Fig. 3), can be expressed as:

$$\frac{\rm S}{\rm I_{reader}}\simeq\frac{\mathcal{R}^{-2A_2}}{6D^{-A_2}\mathcal{R}^{-A_2}}=\frac{1}{6\left(\sqrt{3K}\right)^{-A_2}}, \tag{38}$$

reducing the interference from other cell readers by the factor (in dB) of Eq. (37) divided by two.

For a given number of tags and target collision probability, the formulas of section III provide a way to calculate the required $\delta_{\rm omni}$ for omnidirectional reader antenna and the reduced $\delta_{\rm beam}$ when a directional reader antenna is instead used, for given (fixed) target collision probability. Similarly, reduction of δ for given number of tags, given collision probability and total bandwidth can be achieved when more efficient modulation at each tag is utilized, as will be demonstrated in the numerical results section for omnidirectional reader antenna. In that case, the calculated ratio $\delta_{\rm omni}/\delta_{\rm beam}$ above is substituted by the corresponding ratio of required δ's between the two modulation techniques with omnidirectional antenna.

Therefore, reduction of interference within a cell with the use of efficient modulation techniques and/or directive reader antennas can also reduce interference caused by neighboring same-frequency reader cells (*reader collision*) quantified in backscatter radio environments according to the above.

TABLE I
PARAMETERS FOR NUMERICAL RESULTS

$G_0^{\max} P_\Gamma$ = 30 dBm	G_S = 3 dBi	η = -10 dB	
$\mathcal{N}_0$ = -174 dBm/Hz + NF	$\lambda = \frac{1}{3}$ m	R = 10 bps	κ = 0.5
NF = 10 dB	h_H = 3 m	h_S = 0.25 m	$d_{\min}$ = 3.5 m
SLL = -13 dB	$A_1 = 2$	$A_2 = 4$	

V. NUMERICAL RESULTS

The parameters for the numerical experiments are set according to Table I. The sensor antenna is placed close to the ground resulting in a small $d_{\text{th}} = 28.5$ m, according to Eq. (3). This could be the case in backscatter networks of vegetable plants at an agricultural field. The minimum distance $d_{\min}$ is set larger than a value that assures the validity of the far-field power loss equations of section II [18]. The maximum distance $d_{\max}$ is set to a value that provides acceptable thermal noise-limited performance, at the absence of interfering tags ($N = 0$). Specifically, assuming omnidirectional hub antenna and $N = 0$ ($\mathsf{Y} = 1$), the value of $d_{\max} = 65$ m sets outage probability below $\mathbb{P}_{\text{out}} \approx 1\%$ in Eq. (13), for various values of threshold Θ up to 10 dB.

Fig. 4 presents omni hub antenna analysis and simulation results, with $N = 99$ tags, $d_{\max} = 65$ m and two specific values for tag modulating frequency separation, $\delta = 100$ Hz and $\delta = 200$ Hz. Analysis of section III-A and simulation results match. Furthermore, it is shown that doubling δ significantly reduces collision probability, even though collision is not eliminated. The same plot includes the performance floor for a single tag ($N = 0$) and one can see how far away the network operates from the collision-free case. Notice that increasing δ by a factor of 2 doubles the aggregate communication bandwidth required for all sensors. The results are set according to $\nu = 4$ corresponding to continuous phase modulation at each tag, as in MSK. It is noted that if modulation at each tag is changed to $\nu = 2$ (as in ASK or BPSK), then edge collision probability, according to section III-A, reaches $\mathbb{P}_{\text{out}} = 98.3\%$ for $\Theta = 6$ dB and $\mathbb{P}_{\text{out}} = 94.8\%$ for $\Theta = 3$ dB, with $\delta = 200$ Hz.

That result implies that a certain class of modulation schemes might not be appropriate for extended range, high-density, low-bit rate backscatter sensor networks. Intuition suggests that the required extended range of backscatter sensor networking, in combination with the round-trip nature of signal propagation (i.e. from hub to sensor and then backscattered back to the hub), both demand high *dynamic range* operation: the ratio between the stronger and the weakest signal expected from such operation is significantly larger than in systems which operate in shorter distances or by means of conventional (one-way) radio. Such conjecture has been also validated by analysis results of section III-A, Eq. (23): the ratio between smaller and larger distance raised to the appropriate path loss exponent, is raised to the second power, exactly due to the round trip nature of backscatter communication. Therefore, resistance to interference caused by neighboring in subcarrier-frequency tag signals ought to be stronger and thus, spectrum efficient modulation techniques are required, while some common modulation techniques used in conventional radio may not maximize the number of tags (sensors) for given aggregate bandwidth.

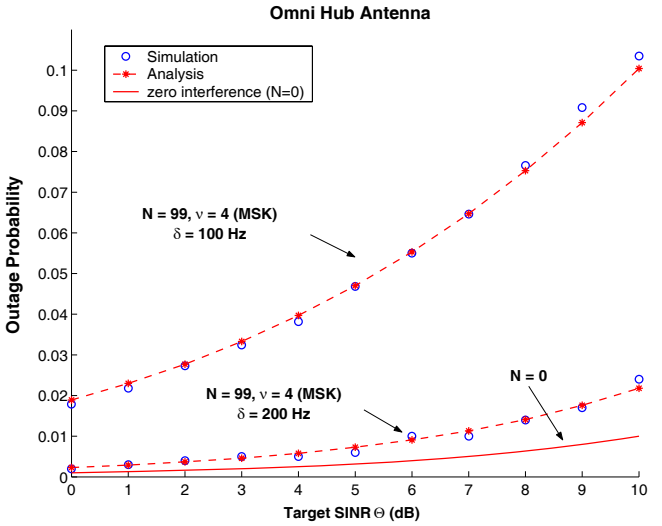

Fig. 4. Analysis match simulation results for two cases of modulating (subcarrier) tag frequency separation δ among 100 tags. Collision-free performance is possible only with appropriate δ and subcarrier modulation.

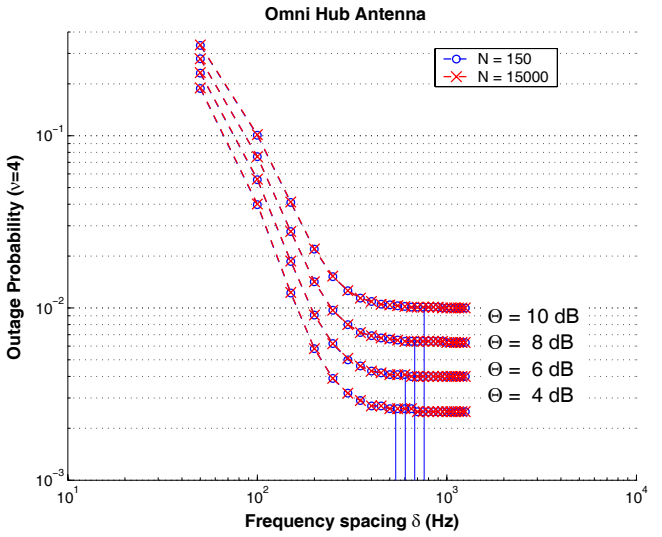

Fig. 5. There exists minimum modulating (subcarrier) tag frequency separation δ that provides acceptable, or collision-free performance (logarithmic horizontal axe) for given modulation at each sensor (ν).

Fig. 5 plots edge collision probability against various values of δ and omnidirectional hub antenna for the same parameters, as in Fig. 4. The first observation is there are values of δ where outage probability approaches the performance of single-tag operation, and collision is eliminated. The same figure plots vertically $5\delta_0$, where δ_0 is the bound calculated from Eq. (23), found on the order of 0.1 kHz. It is shown that frequency separation $5\delta_0$ (on the order of a few hundreds of Hz) provides near collision-free performance. The same bound for $\nu = 2$ (BPSK) suggests prohibitively large δ: specifically, $\delta_0 = 5.15$ kHz for $\Theta = 3$ dB, and $\delta_0 = 7.27$ kHz for $\Theta = 6$ dB, implying that the required modulating frequency separation δ should be on the order of tens of kHz; thus, such modulation ($\nu = 2$) would require two orders of magnitude more aggregate communication bandwidth compared to modulations with $\nu = 4$.

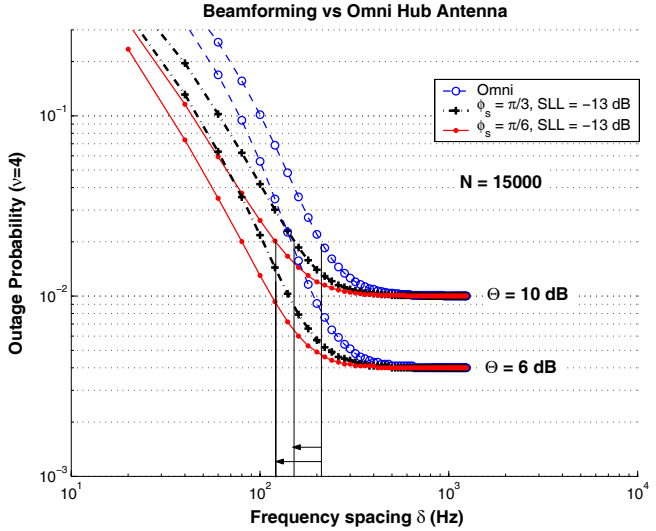

Fig. 6. A moderately directive hub antenna can significantly reduce the minimum modulating tag frequency separation δ (logarithmic horizontal axe).

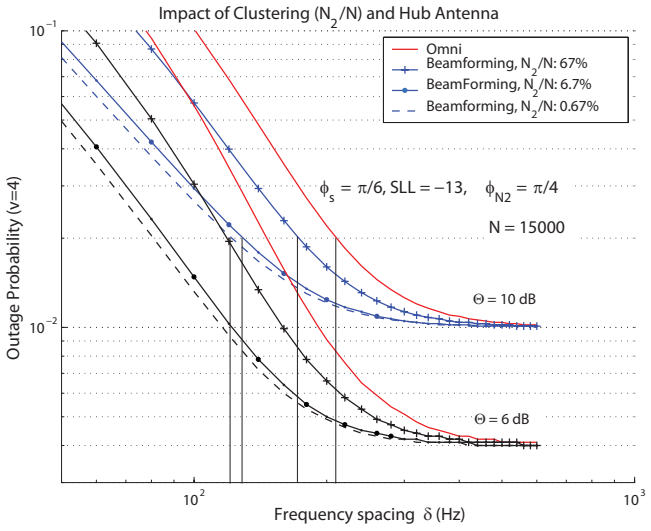

Fig. 7. Impact of clustering of N_2 sensors out of $N = N_1 + N_2$ within a section of angular width $2\phi_{N2}$. Bandwidth savings of a directive hub antenna compared to omni, are depicted as a function of clustering degree N_2/N (logarithmic horizontal axe).

Once again, this finding suggests that acceptable anti-collision performance is feasible only with appropriate modulation at each tag, for given density of tags and available bandwidth.

The second observation is that the plots are identical for two values of large N; that is equivalent to claiming that collision is affected by *neighboring* in subcarrier frequency tags, and not *all* tags. That is true given the fact that aggregate communication bandwidth in this work is proportional to $(N+1)\delta$; increasing the number of tags and the overall required communication bandwidth, keeps tag modulating frequency separation δ constant. From Fig. 5, it is found that for target $\mathbb{P}_{\text{out}} = 2\%$ and $\Theta = 10$ dB, required subcarrier frequency spacing $\delta \simeq 210$ Hz amounts to $(N+1)\delta \simeq 3.1$ MHz, for communication bandwidth of $R = 10$ bps/sensor and ~ 1 tag/m^2 or $N = 15001$.

Fig. 6 shows how such aggregate bandwidth can be reduced by a factor of ~ 5 by means of a directive hub antenna. Specifically, ideal beamforming with a moderate antenna lobe width of $2\phi_S$, $\phi_S = \pi/6$ and SLL=-13 dB, reduces δ by a factor of ~ 5.5. This major improvement might seem surprising, given the moderate value of ϕ_S. Nevertheless, the intuitive explanation is simple: subcarrier (modulating) frequency division in this work amounts to restricting sources of collision to neighboring in subcarrier frequency tags, as shown above. Further utilizing a moderately directive hub antenna pattern, restricts sources of collision to tags which are neighboring in subcarrier frequency *and* bearing angle ϕ. In that way, benefits of frequency and space division are jointly exploited. Implementing in practice directive antennas with moderate main lobe width and moderate SLL, is feasible and relevant designs have been thoroughly studied in the literature (e.g. see utilization of left or right inputs in 4x4 or 8x8 Butler Matrix antennas in [19], [20]).

Fig. 7 repeats the same experiment with $\phi_S = \pi/6$ and SLL=-13 dB, $N = N_1 + N_2 = 15000$, where N_1 sensors are distributed as before, while N_2 sensors are clustered in an angular section of width $2\phi_{\text{N2}} = \pi/2$, for various degrees of clustering N_2/N. Clustering concentrates the sensors in a specific geographic region and therefore reduces the benefits of a directive hub antenna. However, the numerical results for $\Theta = 10$ dB show that a directive hub antenna reduces bandwidth to approximately 60% (compared to omnidirectional hub antenna), even when clustering N_2/N approaches 67%. For smaller clustering degrees, bandwidth savings are larger, as expected. Performance for omnidirectional hub antenna remains the same for the three depicted clustering degrees, since minimum and maximum distance are kept the same for all sensors. It is noted that analysis results of section IV-A are worst-case and can be extended to any clustering degree N_2/N.

Table II summarizes the reduction in total bandwidth, or equivalently the increase in number of supported sensors for given bandwidth, for the two cases of ϕ_S described above. The same table quantifies (in dB) the reduction of interference caused by a distant tag operating at the same *subcarrier* frequency, as well as the reduction of interference caused by a distant reader operating at the same *carrier* frequency, alongside the analysis of section IV-B. The use of a directive antenna at each reader cell reduces the required aggregate bandwidth per cell for given target collision probability and sensor density, and therefore provides opportunities for better frequency reuse, larger reuse distance and consecutively, smaller interference caused by distant reader cells, as explained before.

Subsequently, Fig. 8 studies the case of a non-ideal beamforming hub antenna. Specifically, a three-sector, switched-beam hub antenna is considered, where each sector is covered by a hub antenna with $\phi_S = \pi/9$, $d_{\max} = 54$ m, $\Theta = 10$ dB and $N = 15000$. The new value of maximum distance has been set according to worst case direction ϕ_D of hub antenna: for each main lobe switch, the minimum hub antenna gain for test sensor becomes $G_0(\phi_D - \phi_L)$ (Fig. 1). For the cases depicted, such gain is 3 dB less than maximum antenna gain, and thus maximum distance is set for this worst

TABLE II
INTER-CELL COLLISION REDUCTION

	$\frac{\delta(\text{omni})}{\delta(\phi_S = \pi/3)}$	$\frac{\delta(\text{omni})}{\delta(\phi_S = \pi/6)}$
$(\mathbb{P}_{\text{out}} = 2\%,\ \Theta = 10$ dB)	2.4	5.5
$\left(\frac{S}{I_{\text{tag}}}\right)_{\text{gain}}$	15 dB	29 dB
$\left(\frac{S}{I_{\text{reader}}}\right)_{\text{gain}}$	7.5 dB	14.5 dB

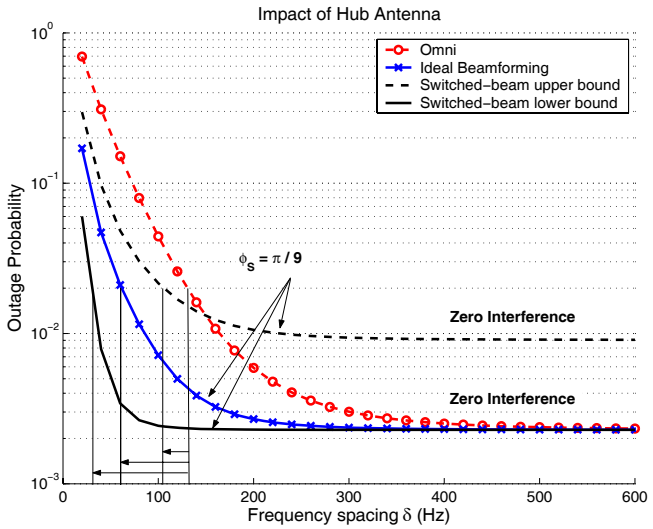

Fig. 8. Bandwidth reduction for the case of non-ideal, beamforming hub antenna with $\phi_S = \pi/9$ and SLL $= -13$ dB (corresponding to 8×8 Butler matrix antenna design found in [19]).

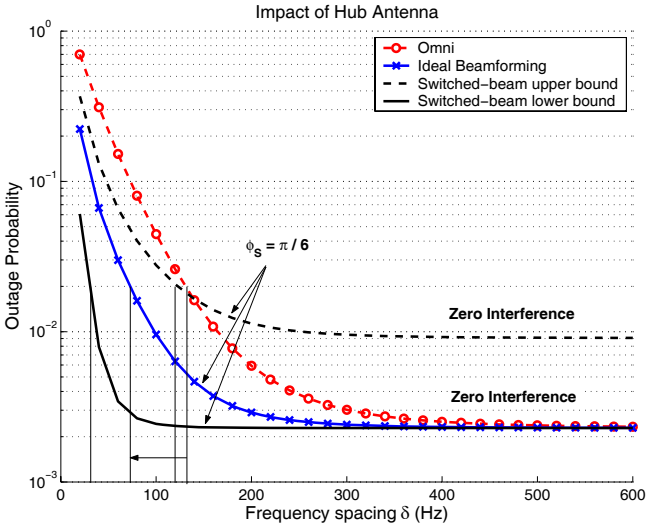

Fig. 9. Bandwidth reduction for the case of non-ideal, beamforming hub antenna with $\phi_S = \pi/6$ and SLL $= -13$ dB (corresponding to 4×4 Butler matrix antenna design found in [19]).

case gain to provide zero-interference ($N = 0$), noise-limited performance slightly below $\mathbb{P}_{\text{out}} = 1\%$. Notice that such worst-case assumption sets an upper bound for the noise-limited error floor, as in principle the test tag is "illuminated" with higher gain.

For both noise and interference-limited performance $\mathbb{P}_{\text{out}} = 2\%$, it is shown that aggregate communication bandwidth $W_{\text{tot}} \propto (N+1)\delta$ can be reduced compared to the omnidirectional antenna case, or equivalently, the total number of sensors can be increased for given bandwidth. Such improvement is quantified by an approximate factor between $1.3 - 4.3$ according to the calculated bounds. The factor is closer to ~ 2.2 which corresponds to the ideal beamformer. For a large network of low-bit rate tags (e.g. $N = 15000$ corresponding to approximately 1.6 sensors/m^2 for the examined scenario), the required aggregate bandwidth is also large, and thus such bandwidth reduction becomes very important. The same plot shows that when interference is not an issue, performance upper bound is affected by ϕ_L; as expected, when performance is thermal noise limited only, hub antenna gain is limited by $G_0(\phi_D - \phi_L)$ and affects received power p_0 by a factor of $G_0(\phi_D - \phi_0)^2$. Therefore, it is important to have a directive antenna (small ϕ_S) with large $G_0(\phi_D - \phi_L)$. Finally, Fig. 9 repeats the same experiment as above, for a hub antenna with $\phi_S = \pi/6$. Given that ϕ_S is slightly larger (antenna less directive), performance gains are slightly smaller, as expected.

Practical design of a hub antenna with SLL and main lobe width $2\phi_S$ parameters similar to experiments of Fig. 8 and Fig. 9 can be performed with a 8x8 and a 4x4 Butler Matrix respectively. Specifically, the design of a 4x4 or 8x8 Butler Matrix antenna with main lobe width $2\phi_S$ and SLL close to the values used above, is studied in [19] with appropriate utilization of the antenna feeding network inputs (e.g. see Fig. 7b and Fig. 10a for 4x4 and 8x8 respectively, in [19]). Practical design of the feeding network for a Butler Matrix reader (hub) antenna is discussed in [21]. It is noted again that other antenna designs with similar values are possible, given the broad antenna model adopted in this work and explained in section II.

VI. CONCLUSION

Acceptable anti-collision performance can be engineered in high-density, low-bit rate backscatter sensor networks, provided that special attention is given on the modulation utilized at each sensor. The round-trip nature and extended range of proposed BSNs result in a more difficult "near-far" problem and demand operation at higher *dynamic range* than conventional radio. As a result, only specific modulation techniques may be appropriate for given aggregate bandwidth and total number of sensors. Analytical results are general enough to cover various modulation techniques (parameter ν), propagation loss exponents ($0 < A_1 < A_2$), as well as antenna directivity patterns. Furthermore, significant gains in aggregate bandwidth or total number of sensors can be engineered with acceptable anti-collision performance, when a moderately directive reader antenna is utilized. It is important to note that that the strategy used in this work to alleviate *tag* collision also assists *reader* collision mitigation. That is due to the fact that bandwidth reduction per reader, for given anti-collision performance, amounts to better frequency reuse among various readers and larger reuse distance.

APPENDIX
INDEFINITE INTEGRAL CLOSED FORM

Theorem 1:

$$g_1(y;\Theta,2A)=\int\frac{1}{1+\Theta\ y^{-2A}}\,dy \tag{39}$$
$$=\begin{cases} y-y\ {}_2F_1\left(\frac{1}{2A},1;1+\frac{1}{2A};-\frac{y^{2A}}{\Theta}\right), & |\Theta\ y^{-2A}|>1,\\ y\ {}_2F_1\left(-\frac{1}{2A},1;1-\frac{1}{2A};-\frac{\Theta}{y^{2A}}\right), & |\Theta\ y^{-2A}|<1,\\ y/2, & \Theta\ y^{-2A}=1,\end{cases}$$

where

$${}_2F_1\left(a,b;c;z\right)\triangleq\frac{\Gamma(c)}{\Gamma(a)\Gamma(b)}\sum_{n=0}^{+\infty}\frac{\Gamma(a+n)\Gamma(b+n)}{\Gamma(c+n)}\frac{z^n}{n!}$$

is the Gauss hypergeometric function and $\Gamma(z)=\int_0^\infty t^{z-1}e^{-t}dt$ is the Gamma (Factorial) function [17].

Proof: For $\Theta\ y^{-2A}=1$ the integrated function becomes $\frac{1}{2}$ and thus, the integral result becomes $\frac{y}{2}$.

For $|\Theta\ y^{-2A}|<1$, the derivative of Eq. (39) right-hand-side (RHS) becomes:

$$(\text{RHS})'=$$
$$=\frac{\Gamma(1-\frac{1}{2A})}{\Gamma(1)\Gamma(-\frac{1}{2A})}\sum_{n=0}^{+\infty}\frac{\Gamma(1+n)\Gamma(-\frac{1}{2A}+n)}{\Gamma(1-\frac{1}{2A}+n)}\frac{\left(-\Theta\ y^{-2A}\right)^n}{n!}+$$
$$+\ y\ \frac{\Gamma(1-\frac{1}{2A})}{\Gamma(1)\Gamma(-\frac{1}{2A})}\sum_{n=1}^{+\infty}\frac{\Gamma(1+n)\Gamma(-\frac{1}{2A}+n)}{\Gamma(1-\frac{1}{2A}+n)}\times$$
$$\times\frac{n}{n!}\left(-\Theta\ y^{-2A}\right)^{n-1}(-\Theta)(-2A)y^{-2A-1} \tag{40}$$
$$=1+\frac{\Gamma(1-\frac{1}{2A})}{\Gamma(1)\Gamma(-\frac{1}{2A})}\sum_{n=1}^{+\infty}\frac{\Gamma(1+n)\Gamma(-\frac{1}{2A}+n)}{\Gamma(1-\frac{1}{2A}+n)}\times$$
$$\times(1-2An)\frac{\left(-\Theta\ y^{-2A}\right)^n}{n!} \tag{41}$$
$$\overset{(a)}{=}1-\frac{1}{2A}\sum_{n=1}^{+\infty}\frac{1}{n-\frac{1}{2A}}(1-2An)\left(-\Theta\ y^{-2A}\right)^n$$
$$=1+\sum_{n=1}^{+\infty}\left(-\Theta\ y^{-2A}\right)^n\overset{(b)}{=}\frac{1}{1+\Theta\ y^{-2A}}, \tag{42}$$

where we have used in (a) the fact that $\Gamma(1+z)=z\Gamma(z)$ and $\Gamma(n+1)=n!$ [17] and in (b) the fact that $|\Theta\ y^{-2A}|<1$.

Working similarly for $|\Theta\ y^{-2A}|>1$, the derivative of Eq. (39) right-hand-side (RHS) becomes:

$$(\text{RHS})'=$$
$$=1-\sum_{n=0}^{+\infty}\frac{1}{1+2An}\left(-\frac{1}{\Theta}\ y^{2A}\right)^n-\sum_{n=1}^{+\infty}\frac{1}{1+2An}\times$$
$$\times\ 2An\left(-\frac{1}{\Theta}\ y^{2A}\right)^n \tag{43}$$
$$=-\sum_{n=1}^{+\infty}\left(-\frac{1}{\Theta}\ y^{2A}\right)^n\overset{(c)}{=}\frac{\Theta^{-1}y^{2A}}{1+\Theta^{-1}y^{2A}}=\frac{1}{1+\Theta\ y^{-2A}}, \tag{44}$$

where we have used in (c) the fact that $|\frac{1}{\Theta}\ y^{2A}|<1$, completing the proof. ■

REFERENCES

[1] H. Stockman, "Communication by means of reflected power," in *Proc. IRE*, pp. 1196-1204, 1948.

[2] J. Paradiso, K. Hsiao, and A. Benbasat, "Tangible music interfaces using passive magnetic tags," in *Proc. ACM Conf. Human Factors Computing Systems: Special Workshop New Interfaces Musical Expression (CHI 2001)*. ACM Press, 2001.

[3] J. Paradiso, L. Pardue, K. Hsiao, and A. Benbasat, "Electromagnetic tagging for electronic music interfaces," *J. New Music Research*, vol. 32, no. 4, pp. 395-409, Dec. 2003.

[4] G. Vannucci, A. Bletsas, and D. Leigh, "Implementing backscatter radio for wireless sensor networks," in *Proc. IEEE Personal, Indoor Mobile Radio Commun.*, Sept. 2007, pp. 1-5.

[5] ——, "A software-defined radio system for backscatter sensor networks," *IEEE Trans. Wireless Commun.*, vol. 7, no. 6, pp. 2170-2179, June 2008.

[6] D. M. Dobkin and T. Wandinger, "A radio-oriented introduction to RFID–protocols, tags and applications," *High Frequency Electron.*, pp. 32-46, Aug. 2005.

[7] J. Banks, D. Hanny, M. A. Pachano, and L. G. Thompson, *RFID Applied*. John Wiley and Sons, 2007.

[8] G. D. Durgin and A. Rohatgi, "Multi-antenna RF tag measurement system using back-scattered spread spectrum," in *Proc. IEEE RFID Conf.*, Las Vegas, NV, Apr. 2008.

[9] M. Chuang and W. H. Shaw, "RFID: integration stages in supply chain management," *IEEE Eng. Manag. Rev.*, vol. 35, no. 2, 2007.

[10] P. V. Nikitin and K. Rao, "Theory and measurement of backscattering from RFID tags," *IEEE Antennas Propagat. Mag.*, vol. 48, no. 6, Dec. 2006.

[11] P. V. Nikitin, K. Rao, and R. Martinez, "Differential RCS of RFID tag," *Electron. Lett.*, vol. 43, no. 8, Apr. 2007.

[12] W. C. Jakes, Ed., *Microwave Mobile Communications*. New York: IEEE Press, 1974.

[13] D. Cassioli, M. Z. Win, and A. F. Molisch, "The ultra-wide bandwidth indoor channel: from statistical model to simulations," *IEEE J. Select. Areas Commun.*, vol. 20, no. 6, pp. 1247-1256, Aug. 2002.

[14] D. Kim, M. A. Ingram, and W. W. Smith, "Measurements of small-scale fading and path loss for long range RF tags," *IEEE Trans. Antennas Propagat.*, vol. 51, no. 8, pp. 1740-1749, Aug. 2003.

[15] J. D. Griffin and G. D. Durgin, "Gains for RF tags using multiple antennas," *IEEE Trans. Antennas Propagat.*, vol. 56, no. 2, pp. 563-570, Feb. 2008.

[16] S. Benedetto, E. Biglieri, and V. Castellani, *Digital Transmission Theory*. Prentice-Hall, 1987.

[17] M. Abramowitz and I. A. Stegun, *Handbook of Mathematical Functions wih Formulas, Graphs, and Mathematical Tables*. Washington, DC: United States Department of Commerce, 1970.

[18] C. A. Balanis, *Antenna Theory: Analysis and Design*. John Wiley and Sons, 2005.

[19] E. Siachalou, E. Vafiadis, S. S. Goudos, T. Samaras, C. S. Koukourlis, and S. Panas, "On the design of switched-beam wideband base stations," *IEEE Antennas Propagat. Mag.*, vol. 46, no. 1, pp. 158-167, 2004.

[20] G. Miaris, E. Siachalou, T. Samaras, S. Goudos, E. Vafiadis, and S. Panas, "On mobile communications smart base-station system design," *IEEE Antennas Propagat. Mag.*, vol. 47, no. 2, pp. 139-144, 2005.

[21] E. Vaitsopoulos, A. Bletsas, and J. N. Sahalos, "On the RFID design with passive tags and a butler matrix reader," in *Proc. IEEE 13th Biennial Conf. Electromagnetic Field Computation*, May 2008.

Aggelos Bletsas (S'03–M'05) received with excellence his diploma degree in Electrical and Computer Engineering from Aristotle University of Thessaloniki, Greece in 1998, and the S.M. and Ph.D. degrees from Massachusetts Institute of Technology in 2001 and 2005, respectively. He worked at Mitsubishi Electric Research Laboratories (MERL), Cambridge MA, as a Postdoctoral Fellow and at Radiocommunications Laboratory (RCL), Department of Physics, Aristotle University of Thessaloniki, as a visiting scientist. He joined Electronic and Computer Engineering Department, Technical University of Crete, in summer of 2009, as an Assistant Professor.

His research interests span the broad area of scalable wireless communication and networking, with emphasis on relay techniques, signal processing for communication, radio hardware/software implementations for wireless transceivers and low cost sensor networks, RFID, time/frequency metrology and bibliometrics.

Dr Bletsas, received best undergraduate thesis award from Ericsson Hellas for the development of a complete Text-to-Speech system for the Greek Language, commercialized in 1999. He received awards for undergraduate excellence from Technical Chamber of Greece and State Scholarship Foundation (IKY). During his graduate studies at MIT, he was supported by fellowship awards from BT and Nortel Networks. Dr. Bletsas was the co-recipient of IEEE Communications Society 2008 Marconi Prize Paper Award in Wireless Communications.

Stavroula Siachalou received the Diploma degree in Electrical & Computer Engineering (ECE) from Aristotle University of Thessaloniki (AUTH), Greece, in 2000. Five years later she completed her Phd studies at the ECE Department of AUTH, in the area of algorithmic computing, QoS provisioning, routing and multicast communication. Since 2006 she is with the General Directorate of Technical Services and Computerization of AUTH. Since 2000 she has been working in various research projects dealing with QoS routing, radio communications and machine translation. Her interests are in the area of wireless communications, QoS provisioning, routing, shceduling, modeling and performance analysis, multicast and sensor netwoking.

John N. Sahalos (M'75-SM'84-F'06) was born in Philippiada, Greece. He carried out all his University studies in Greece where he received from 1967-75 his B.Sc. degree in Physics, his Diploma in Civil Engineering, and his M.Sc. and Ph.D. degrees in Electronic Physics from the Aristotle University of Thessaloniki (AUTh).

After working as a Postdoctoral University Fellow (1976) at the ElectroScience Laboratory of the Ohio State University in USA, he was elected, (1977), Professor of Microwaves at the School of Engineering at the University of Thrace, Greece. After that he was elected, (1985), Professor of Antennas & Microwaves at the AUTh, where he serves till now. He was a visiting Professor at the University of Colorado, Boulder, USA, (1982-1983) and at the Technical University of Madrid, Spain, (1989-1990).

Professor Sahalos was a supervisor in 24 PhDs and in more than 100 MSc theses. He is the Director of Post-Graduate Studies in Electronic Physics at AUTh. He is the Director of a Laboratory Network (five Labs / three from Academy and two from Industry), for Certification and Testing of Telecommunication Terminals. He is the President of the ICT Committees of the National Council for Research & Technology. He is the national representative and President of URSI. He is the Vice-president of the ICT Net at AUTh. He is the vice-president of the Research Committee of AUTh (2007-2010). He was a member of the Board of Directors of OTE S.A. (2002-04). He is a member of EEF, URSI, IEEE and the Technical Chamber of Greece. Moreover, he has been a member of assessment committees for the evaluation of scientific papers and research proposals, at an international level.

He is a consultant to industry, both in Greece and abroad. He has an extensive record of publications, (more than 350), in international scientific journals and conferences. He is the author of four textbooks (one in English, three in Greek) and seven book chapters. He has participated in chairing and organizing various international conferences and symposia. He was involved in more than 50 research projects in Greece and abroad as a project manager. His primary research deals with antennas, microwave engineering, biomedical engineering, EMC and radio-communications.

Professor Sahalos was elected as an IEEE Fellow for his Contributions in Antenna Analysis & Design. He received three Awards for his scientific works and two Service Excellence Awards. He also honored from the Ministerio de Education Y Ciencia, Spain.